Biosensors and Bioelectronics 59 (2014) 192–199

Contents lists available at ScienceDirect

Biosensors and Bioelectronics

journal homepage: www.elsevier.com/locate/bios

Real-time analysis of the effects of toxic, therapeutic and sub-therapeutic concentrations of digitoxin on lung cancer cells

R. Eldawud [a], T.A. Stueckle [b,d], S. Manivannan [a], H. Elbaz [c], M. Chen [d], Y. Rojanasakul [d,e,*], C.Z. Dinu [a,d,e,**]

[a] Department of Chemical Engineering, West Virginia University, WV, United States
[b] Health Effects Laboratory Division, National Institute for Occupational Safety and Health, WV, United States
[c] Wayne State University School of Medicine, MI, United States
[d] Department of Basic Pharmaceutical Sciences, West Virginia University, WV, United States
[e] Mary Babb Randolph Cancer Center Allen Lung Program, West Virginia University, WV, United States

ARTICLE INFO

Article history:
Received 10 January 2014
Received in revised form
9 March 2014
Accepted 12 March 2014
Available online 26 March 2014

Keywords:
Digitoxin
Cell-based sensing
Cell adhesion
Anti-cancer

ABSTRACT

Digitoxin belongs to a naturally occurring class of cardiac glycosides (CG); digitoxin is clinically approved for heart failure and known for its anti-cancer effects against non-small lung cancer cells (NSCLC). However, concerns associated with its narrow therapeutic index and its concentration-dependent mechanism of action are rising. Thus, before digitoxin implementation in designing and developing safer and more effective CG-based anti-cancer therapies, its pharmacological and safety profiles need to be fully elucidated. In this research we used a combinatorial approach to evaluate the anti-cancer mechanisms of digitoxin in real-time. Our approach employed a non-invasive electric cell impedance sensing technique as a proxy to monitor NSCLC behavior post-exposure to toxic, therapeutic and sub-therapeutic concentrations of the drug. By developing structure–function combinatorial relations we showed that digitoxin targets cancer cells in a time and dose-dependant manner by activating pro-apoptotic and anti-proliferative signaling cascades that results in strengthening cellular adhesion and sequestration of key regulatory proliferation protein from the nucleus.

1. Introduction

Digitoxin is a natural occurring cardiac glycoside (CG) (Elbaz et al., 2012a) with a prolonged half-life, a well-established clinical profile, a narrow therapeutic window (Elbaz et al., 2012a), and increased ability to readily cross both the blood brain and the placental barriers (Storstein et al., 1979). Laboratory investigations suggested that digitoxin exhibits high selectivity towards cancer cells when compared to healthy cells (Elbaz et al., 2012a; López-Lázaro et al., 2006) making the drug a viable chemotherapeutic alternative against several types of cancer from leukemia, to pancreatic and lung cancers (López-Lázaro, 2007; Winnicka et al., 2006).

The anti-cancer mechanisms induced by digitoxin have been extensively studied and are mainly associated with the drug's ability to manipulate intracellular ion hemostasis which led to a downstream signaling cascade eventually inducing apoptosis and cell cycle arrest (Elbaz et al., 2012b). In particular, *in vitro* studies showed that exposure of non-small lung cells, renal, pancreatic and breast cells to micromolar concentrations of digitoxin (0.5–5 μM) inhibits Na^+/K^+-ATPase pump activity (López-Lázaro, 2007; Newman et al., 2008), induces calcium-dependent activation of caspases and other hydrolytic enzymes (Einbond et al., 2008; Elbaz et al., 2012a), causes generation of reactive oxygen species (Prassas et al., 2011), activates the cell-cycle inhibitor p21Cip1 (Prassas et al., 2011), directs the inhibition of topoisomerase activity and hypoxia-inducible factor1a synthesis (Sun et al., 2013), and ultimately reduces viability and cell proliferation (Elbaz et al., 2012a; Menger et al., 2013). Complementary, cellular exposure to nanomolar concentrations of digitoxin (10–100 nM) leads to inhibition of (HIF-1) and topoisomerase II synthesis (Prassas et al., 2011), activation of phospholipase C (Elbaz et al., 2012a; Ho et al., 1987), phosphatidylinositol-3-kinase (PI3K)

* Corresponding author at: Department of Basic Pharmaceutical Sciences, West Virginia University, PO Box 9530, Morgantown, WV 26505, USA.
Tel.: +1 304 293 1476; fax: +1 304 293 2576.
** Corresponding author at: Department of Chemical Engineering, Benjamin M. Statler College of Engineering and Mineral Resources, West Virginia University, PO Box 6102, Morgantown, WV 26506, USA.
Tel.: +1 304 293 9338; fax: +1 304 293 4139.
E-mail addresses: yrojan@hsc.wvu.edu (Y. Rojanasakul), cerasela-zoica.dinu@mail.wvu.edu (C.Z. Dinu).

http://dx.doi.org/10.1016/j.bios.2014.03.030
0956-5663/

(Ho et al., 1987), tyrosine kinase (Src) (Elbaz et al., 2012a; Jagielska et al., 2009), mitogen-activated protein kinase (MAPK) (Prassas et al., 2011), affects cell cycle and anoikis (Pongrakhananon et al., 2014) inducing alternations in membrane fluidity (Larre et al., 2010; Xie and Cai, 2003), ultimately leading to cell apoptosis (Lopez-Lazaro et al., 2005). However, the nature of these *in vitro* studies only allowed for discrete time points monitoring and limited analysis of the cellular functions upon exposure, all after invasive or destructive preparation of the samples, as well as labor intensive and time consuming analysis. Therefore, further studies are needed to better characterize the pharmacological and safety profiles of digitoxin before its chemotherapeutic implementation, especially considering that therapeutic concentrations of digitoxin varies according to the age and weight of the patient, generally ranging from 26 to 46 nM (Wu et al., 2001). Such studies do not only have to account for the narrow therapeutic window or drug's dose-dependent and selective apoptosis to cancer cells (Newman et al., 2008; Xie and Cai, 2003), but also need to allow monitoring of the cellular systems without lag time between sample collection and data analysis.

Electric cell–substrate impedance sensing (ECIS) is a non-invasive and quantitative form of cell-based sensing that utilizes identical small gold-film electrodes deposited on the bottom of cell culture dishes to measure the cellular resistance and its alteration upon changes in cell morphology, spreading, attachment and migration (Arndt et al., 2004; Spegel et al., 2008), all as a function of applied frequencies and in real-time (Giaever and Keese, 1984; Wegener et al., 2000a). The applicability of ECIS was extended to inhibition assays for cytochalasin-D (cytoskeletal inhibitor) (Sapper et al., 2006), prostaglandin E2 (inflammatory mediator) (Wang et al., 1995), bacterial protease (Itagaki et al., 2011), or platelet-activating factors that affect in cellular adhesion (Melnikova et al., 2009).

By combining standard *in vitro* cell viability and cell-based cytotoxicity assays with ECIS, we aim to investigate the anti-proliferative and pro-apoptotic mechanisms of non-small lung cancer cells (NSCLC) exposed to different concentrations of digitoxin in real-time. NCI-H460 cells were chosen as model NSCLC based on their sensitivity to digitoxin (López-Lázaro, 2007; Wang et al., 2010) and increased resistance to chemotherapy (Mijatovic et al., 2006a,b). We hypothesized that NCI-H460 exposure to toxic (80 nM), therapeutic (40 nM) and sub-therapeutic (25 and 10 nM) concentrations of digitoxin is associated with changes in the cellular viability that can be monitored using an individual cell as a primary transducer and recording its real-time alterations in morphology and adhesion profile. Further, based on the key role of the cyclin-dependent kinase-4 (CDK4) in regulation of cell proliferation and cell cycle (Gulappa et al., 2013; Si and Liu, 2001), we hypothesized that exposure to digitoxin targets cellular adhesion pathways in a dose and time-dependent manner by sequestering CDK4 in the cytoplasm and thus reducing its nuclear levels. Further, CDK4 association with viable candidates responsible for cellular junctions formation can be monitored in real-time as a change in the cellular attachment profile. Our findings underscore the potential of digitoxin to be used as the next generation of chemotherapeutic drugs that target cell adhesion and cell cycle profiles for improved anti-cancer activity.

2. Materials and methods

2.1. Cell culture and treatment

Human lung cancer epithelial cells (NCI-H460; ATCC, VA) were cultured in Roswell Park Memorial Institute-1640 medium (RPMI-1640; Sigma Chemicals, MO) supplemented with 10% fetal bovine serum (FBS; Atlanta Biologicals, GA), 2 mM L-glutamine and 100-units/mL penicillin/streptomycin (Sigma Chemicals, MO) and maintained in a humidified atmosphere at 37 °C under 5% CO_2. Cells were passaged regularly using 0.25% (w/v) trypsin (Molecular Probles, OR) with 1.5 mM ethylene diaminetetracetic acid (EDTA; Molecular Probles, OR). Stock concentrations of digitoxin (Sigma Chemicals, MO) were made in dimethyl sulfoxide (DMSO; Sigma Chemicals, MO) and diluted to 1000x exposure concentrations as previously described (Elbaz et al., 2012b). Digitoxin exposure was performed in a medium containing 1% FBS, 2 mM L-glutamine and 100-units/mL penicillin/streptomycin. The concentration of FBS was reduced due to existing concerns regarding digitoxin's interaction with serum proteins (Baggot and Davis, 1973) and to better approximate the minimum concentrations and times that were required to achieve drugs' activity *in vitro* (Elbaz et al., 2012b).

2.2. Apoptosis assay

Cells were seeded overnight in 12-well plates (Fisher, PA) at 2×10^5 cell/mL and treated with 0, 10, 25, 40 and 80 nM digitoxin for 24, 48 and 72 h respectively. After treatment, the cells were incubated with 10 μg/mL Hoechst-33342 (Molecular Probles, OR) for 30 min. The percentage of cells having intensely condensed chromatin and/or fragmented nuclei was scored using fluorescence microscope (Leica Microsystems, IL). Approximately 1000 nuclei from ten random fields were analyzed for each sample. The apoptotic percentage was calculated as the percentage of cells with apoptotic nuclei over the total number of cells per field of view.

2.3. Western blot analysis

Cells were seeded overnight in 6-well plates at a density of 6×10^5 cell/well, and treated with 0, 10 or 25 nM digitoxin in 0.1% DMSO for 24 h. Subsequently, cells were placed on ice and lysed for 30 min in a lysis buffer containing 2% Triton X-100, 1% sodium dodecyle sulfate (SDS), 100 mM sodium chloride (NaCl), 10 mM tris-hydrochloric acid (HCl), complete mini cocktail protease inhibitors (all reagents are purchased from Roche, IN) and 1 mM EDTA insoluble cellular debris was pelleted by centrifugation at 4 °C and 16,000 × *g* for 15 min. The supernatant was collected and used to determine the total protein content using standard Bicinchoninic Acid Assay (BCA, Thermo Scientific, IL). Briefly, working reagent was prepared according to the manufacturer instructions by mixing 50 parts of reagent A with 1 part of reagent B (reagents included with kit). Two μL of each sample was added to a 96-well plate and incubated with 200 μL of the working reagent at 37 °C for 30 min; experiments were performed in duplicates. Control calibration curves were prepared using serial dilutions of standard bovine serum albumin (BSA). Absorbance at 562 nm was recorded on a BioTek 96-plate reader (BioTek, Winooski, VT).

The supernatant was separated by a 10% SDS–PAGE gel and transferred to polyvinylidene fluoride (PVDF) membranes using the iBlot® Dry Blotting System (Invitrogen, CA). Membranes were blocked in 5% skim milk in Tris-buffered saline (TBST, 25 mM Tris–HCl, 125 mM NaCl, and 0.1% Tween-20; Sigma Chemicals, MO) for 1 h at room temperature, and subsequently incubated with anti-CDK4 primary antibody (Cell Signaling, MA) at 4 °C overnight. The membranes were subsequently washed three times in phosphate buffer saline (PBS; Lonza, MD) containing 1% Tween-20 for 10 min each, incubated with horseradish peroxidase-conjugated secondary antibody (Cell Signaling, MA) for 1 h at room temperature, then washed again for three more times each for 10 min in TBST. Finally, the samples were analyzed by chemiluminescence

(Supersignal West Pico, IL). Band quantification via densitometry was performed using ImageJ software, version 10.2.

2.4. Trypan-blue exclusion assay

NCI-H460 cells were seeded overnight in 12-well plates at a density of 2×10^5 cell/mL, and treated with 0, 10, 25, 40 or 80 nM digitoxin for 24, 48, and 72 h, respectively. Cells were subsequently washed with PBS, trypsinized (0.25%), suspended in 10% media and stained with 0.4% trypan-blue (Invitrogen, CA) at 1:1 volume ratio and analyzed using Countess automated cell counter (Invitrogen, CA).

2.5. Electric cell–substrate impedance sensing (ECIS)

Real-time quantification of cellular behavior was conducted using an electric cell impedance sensing instrument (ECIS-ZΘ, Applied Biophysics, NY). In one set of experiments, two ECIS arrays (8W10E+), each containing 8-wells with 40 gold electrodes, were simultaneously employed to provide concomitant measurements of 16 samples at multiple frequencies. Prior to any experiment, the gold electrodes were stabilized for 3 h in 400 μl RPMI media to account for electrode variances and to create a reference line associated with free electrodes; subsequently, the array holder was placed in a humidified incubator at 37 °C and 5% CO_2 to provide optimal conditions for cellular growth. NCI-H460 cells were added at a density of 2×10^5 cell/mL in a volume of 400 μl/well. Cells were allowed to settle and grow over the gold electrodes and form a confluent monolayer for 24 h. The formation of the cellular monolayer was indicated as a settlement in the resistance value with minor fluctuation caused by cellular micromotion (Arndt et al., 2004; Giaever and Keese, 1991; Wegener et al., 2000a). Upon monolayer formation cells were treated with 0, 10, 25, 40 or 80 nM digitoxin and their cellular behavior was monitored for 48 h post-exposure.

2.6. Statistical analysis

Results are presented as mean ± standard deviation. Experiments (viability, apoptosis and Western blot) were performed in duplicates and repeated at least 3 times. ECIS experiments were performed in duplicates and repeated at least four times, for a total of minimum 8 replicates per dose. Changes in the behavior of the cells (i.e., resistance) were recorded every 180 s for the duration of the experiments with each time point being an average of 16 replicates (2 arrays with 8 wells each). Two-way analysis of variance and unpaired two-tailed Student's *t*-test were performed using JMP 8.0 (SAS Institute) and SigmaPlot 10.0 (Systat Software Inc.). Results were considered significant for $^*p < 0.05$.

3. Results

3.1. Digitoxin induced apoptosis in a time and dose-dependent manner

To evaluate the effects of digitoxin on cellular apoptosis, confluent monolayers of human lung cancer (NCI-H460) cells were exposed to toxic, therapeutic and sub-therapeutic concentrations of digitoxin for 24, 48 and 72 h respectively. Visual inspection of the 24 h exposed cells showed minor differences in their nuclear morphology for the cells treated with 10 nM (5%) and 25 nM (15%) digitoxin when compared to the untreated cells (Fig. 1A). In contrast, the nuclei of the cells treated with 40 and 80 nM digitoxin showed major changes (≥ 50%) in their morphologies, i.e., rounding, swelling, condensation and fragmentation. Such changes are considered early indicators of cellular apoptosis (Furukawa et al., 2007; Yuan et al., 2007).

The percentage of apoptotic cells at 24, 48 and 72 h post-exposure to toxic, therapeutic and sub-therapeutic concentrations of digitoxin is shown in Fig. 1B. Analysis of variance showed that the NCI-H460 apoptosis was both dose and time-dependent. In particular, 24 h after exposure, the cells treated with 10 nM showed no significant changes in their apoptotic percentage; however, increased apoptosis was noticed after 48 and 72 h of digitoxin exposure. Cells exposed to 25, 40 and 80 nM digitoxin exhibited higher apoptosis within first 24 h with a significant increase after 48 and 72 h, respectively. Values for the IC50 (half-inhibition concentration) derivated using a three-parameter sigmoid regression analysis were 43.4–36.6 nM and 31.6 nM at 24, 48 and 72 h post-exposure respectively.

3.2. Digitoxin inhibited cellular proliferation

To study the effects of toxic, therapeutic and sub-therapeutic concentrations of digitoxin on the NCI-H460 cell proliferation, a live cell exclusion assay was performed. The results showed that exposure to digitoxin caused inhibition of cellular proliferation in a dose and time-dependent manner (Fig. 2A). Specifically, no differences relative to controls were noticed 24 h post-exposure for the cells treated with 10 nM digitoxin; however, significant inhibitory effects were observed after 48 (18%) and 72 h (27%) respectively. For the cells treated with 25, 40 and 80 nM digitoxin, the decrease in the live cell counts was significant within the first 24 h with 35%, 54% and 82% respectively. This subsequently increased to 43%, 70% and 99% after 48 h exposure and 70%, 85% and 100% after 72 h, respectively.

Since inhibition of cell proliferation was the major effect 24 h post-exposure to sub-therapeutic concentrations of digitoxin, we also examined the expression of cyclin-dependent kinases-4 (CDK4), a key regulatory protein that controls cellular proliferation and cell cycle progression at the G1/S phase (Gulappa et al., 2013; Si and Liu, 2001). Western blot analysis showed significant decrease in the expression of CDK4 after exposure to both 10 and 25 nM, with a 35% and 60% reduction in the CDK4 expression relative to expression of control β-actin (Fig. 2B and C).

3.3. Real-time cell monitoring using electric cell impedance sensing

Real-time analysis from the time of cell inoculation into the wells, to the formation of a confluent monolayer, and subsequently 48 h post-exposure to toxic, therapeutic and sub-therapeutic concentrations of digitoxin were performed using electric cell impedance sensing (ECIS). Previous studies showed that cells immobilized onto gold electrodes have similar behaviors with their counterparts immobilized onto polystyrene surfaces (Giaever and Keese, 1991; Wegener et al., 2000b). Fig. 3A shows an eight well ECIS array with inter-finger-like arrangement and the current pathways contributing to the resistance measurements. Once the cells spread onto the gold electrodes, their insulating nature of the plasma membrane constricted the current flow in the spaces beneath the basal membrane and the electrode surface as well as in the paracellular spaces between adjacent cells, leading to the recorded resistance (Giaever and Keese, 1991, 1993). Alpha is a function of the distance between the basal membrane and cellular radius according to the following equation:

$$\alpha = R_c(\rho/h)^{0.5}, \quad (1)$$

where ρ represents the specific resistivity of the electrolyte (i.e., culture media) underneath the cells, h represents the distance at which the cells hover above the electrode, and R_c is the cellular radius.

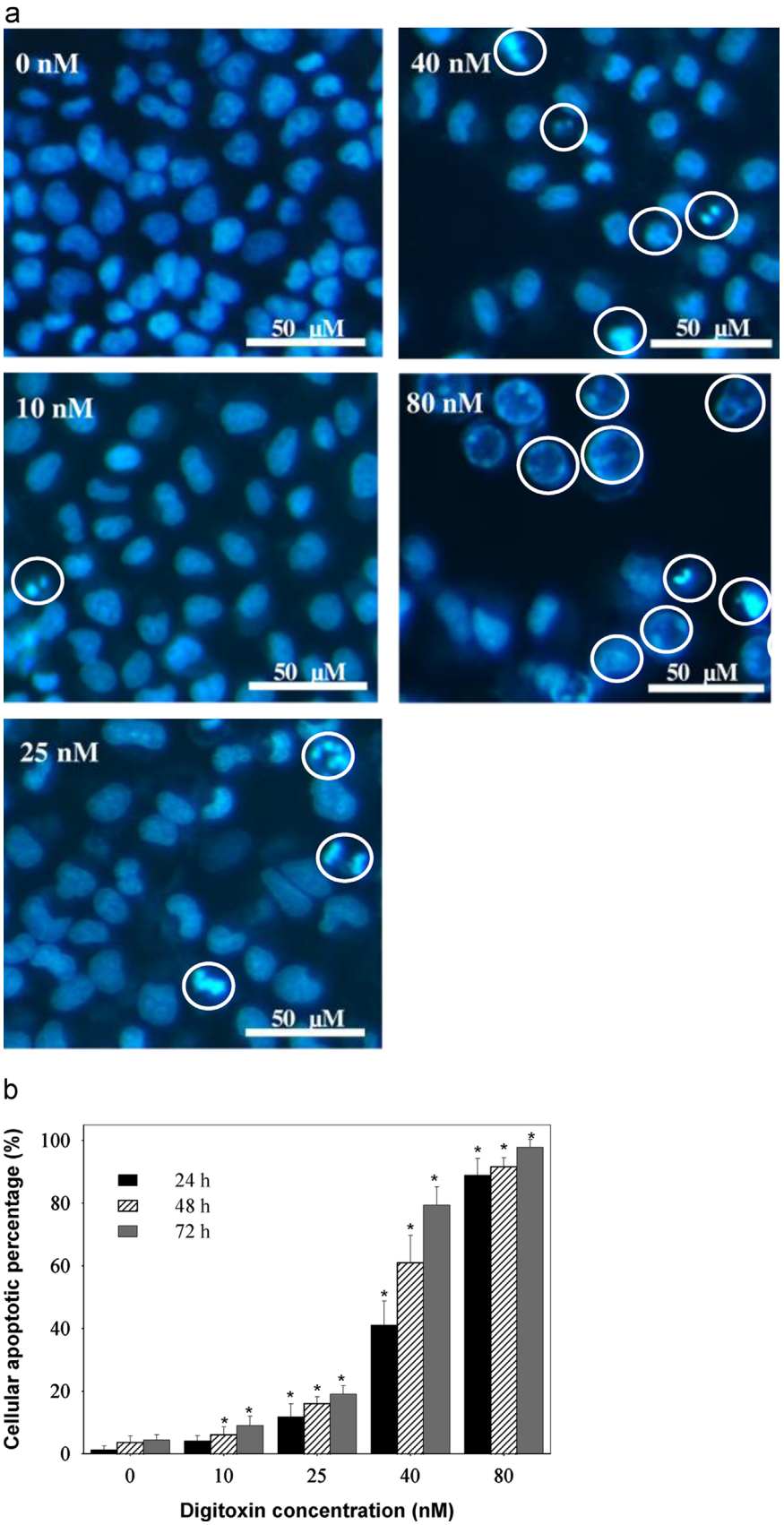

Fig. 1. (A) Fluorescent images of Hoechst stained NCI-H460 cells 24 h post-exposure to digitoxin. Cells treated with 40 and 80 nM digitoxin showed major changes in their nuclei morphologies (white circles) relative to controls or cells treated with 10 and 25 nM digitoxin. (B) Percentage of apoptotic cells upon exposure to digitoxin is dose and time-dependent. Difference is considered significant for $^{*}p < 0.05$.

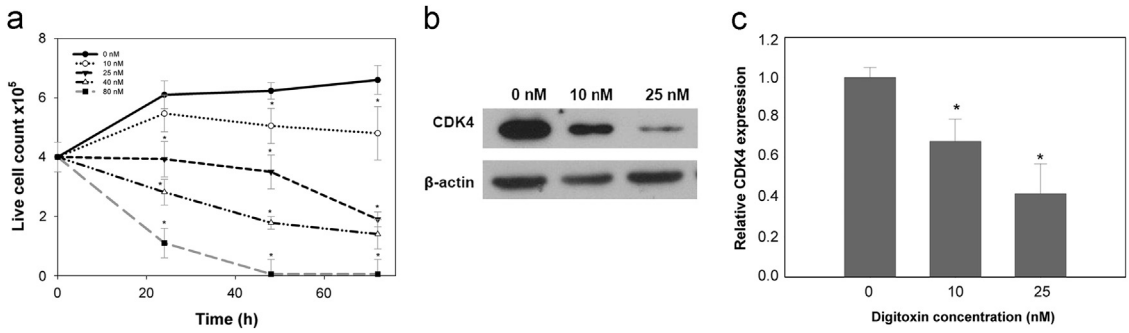

Fig. 2. (A) Live cell counts after 24, 48 and 72 h exposure to different concentrations of digitoxin. (B) Western blot analysis of CDK4 expression relative to control β-actin 24 h post-exposure to digitoxin. (C) Quantification of CDK4 expression levels relative to β-actin. A significant difference is indicated for $^{*}p < 0.05$.

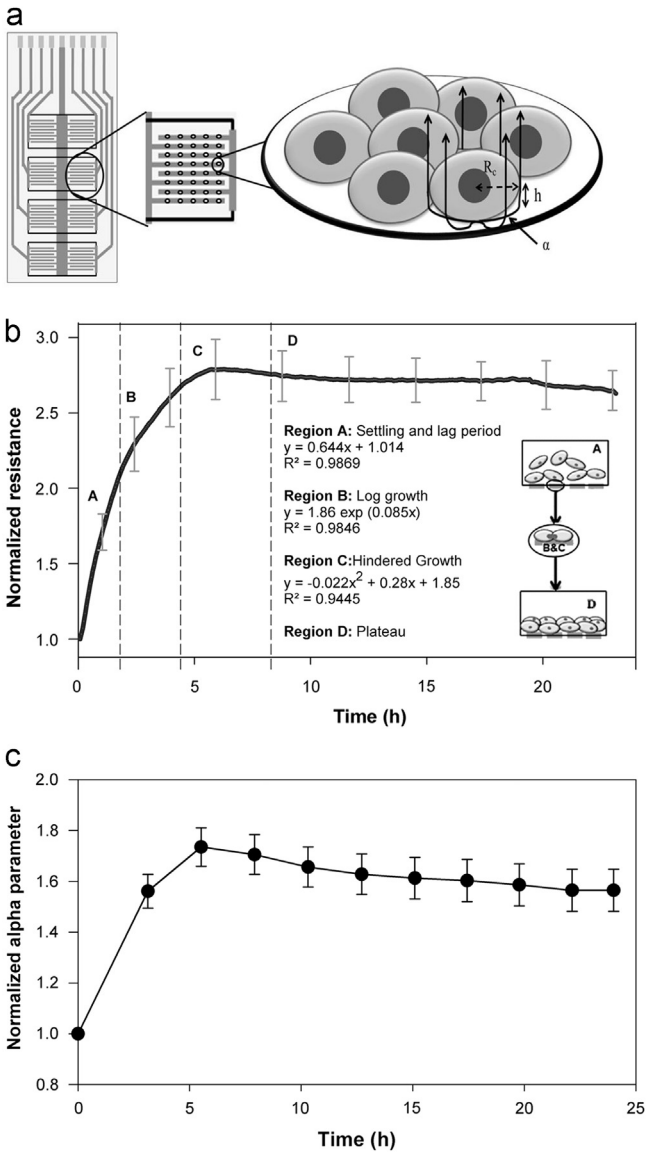

Fig. 3. (A) Schematic illustration of an ECIS array, with a demonstration of the ECIS current pathways accounting for the resistance measurements. (B) Representative real-time measurements of the normalized resistance mathematically modeled according to the growth and spreading behavior of the NCI-H460 cells over the gold electrodes; the standard deviation is shown every two and a half hours and represents an average of 16 measurements (2 arrays with 8 wells each). (C) Real-time changes in α parameter.

The changes in NCI-H460 resistance were mathematically fitted and are shown in Fig. 3B. The monolayer resistance value was normalized to the base level of the cell free electrodes at 4 kHz operational frequency; data was collected every 180 s (Supplementary information Fig. S1). Region A reflects the changes in resistance from inoculation to the cells settling onto the electrodes and includes the lag period or the time required by the cells to overcome the disturbance caused by inoculation. This region was fitted using a linear computational model (Chen et al., 2012; Xiao and Luong, 2005). In particular, for $t < 2$ h

$$R(t) = at + b, \tag{2}$$

where $R(t)$ is the resistance value of the cells setteled onto the electrodes, and a and b are parameters estimated using a least-square algorithm. Region B was directly associated with the cells ability to spread and form increased cell–cell contacts. The starting point for region B was determined by finding the theoretical point where the two mathematical models intercept (i.e., the linear model for region A and the exponential fit for region B respectively). Specifically, for $t \geq \tau$,

$$R(t) = R_1 e^{kt}, \tag{3}$$

where R_1 and k are parameters estimated by the least-square algorithm and τ is the lag period. Using a Taylor's series expansion of a first and second orders, the lag period was found to be 1 h 44 min and 1 h 46 min, respectively, for the NCI-H460 cells. Upon complete coverage of the gold electrodes, cellular proliferation was hindered by contact inhibition shown in region C and modeled using a second order polynomial. Specifically,

$$R(t) = at^2 + bt + c, \tag{4}$$

where $R(t)$ is the resistance of cells the reaching the hindered growth and a, b and c are parameters estimated using the least-square algorithm. Finally, upon the complete formation of cell monolayer, the normalized resistance reached a plateau, i.e., region D.

Cell attachment and monolayer formation was further confirmed by evaluating the changes in α (Arndt et al., 2004; Giaever and Keese, 1991, 1993) (Fig. 3C). An increase in α indicates a decrease in the distance between the gold electrode and the cell basal membrane (h). The results showed that the changes in α followed a similar trend to the changes in the cellular resistance, with no fluctuations being observed after complete formation of the cell monolayer.

Twenty-four hours post-inoculation, the confluent monolayer was exposed to toxic, therapeutic and sub-therapeutic concentrations of digitoxin. Fig. 4A shows the representative normalized resistance of control (untreated) and cells treated with different concentrations of digitoxin as measured every 3 min for a total of

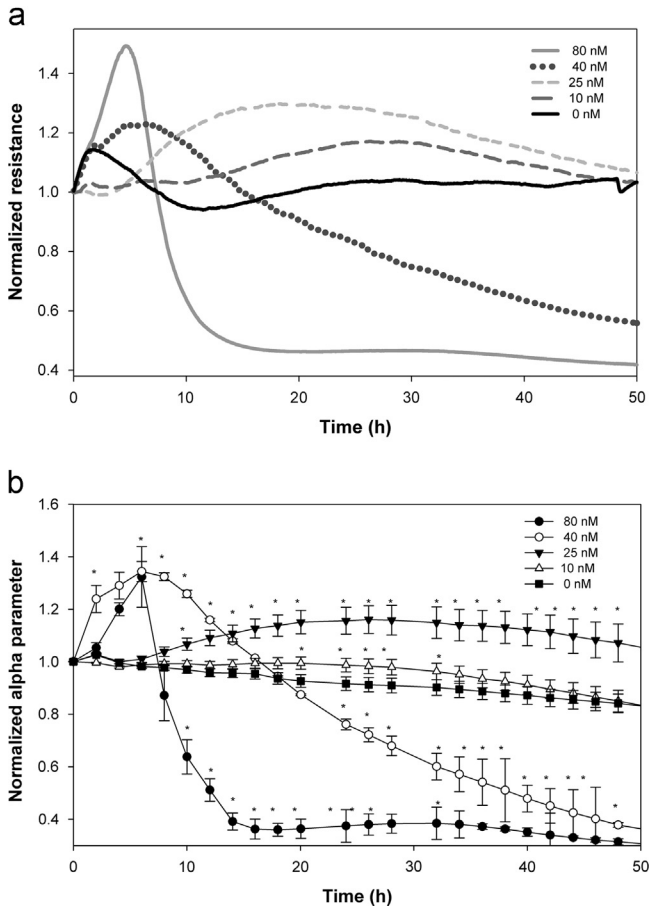

Fig. 4. (A) Representative analysis of the real-time behavior of NCI-H460 cells following digitoxin exposure. (B) Changes in α parameter post-exposure to digitoxin in real-time; * signifies changes considered significant $p < 0.05$.

48 h. An initial increase in resistance with a slower rate for 10 and 25 nM (sub-therapeutic) and a higher rate for both 40 (therapeutic) and 80 nM (toxic) concentrations was recorded. Upon stabilization (~5 h post-exposure), the resistance of the cells exposed to 10 and 25 nM digitoxin showed higher absolute values than the resistance of the controls. Further, the resistance values of the cells treated with 25 nM digitoxin had higher absolute values relative to the absolute values of the 10 nM treated cells. Similarly, the resistance of the cells treated with 40 and 80 nM digitoxin underwent drastic changes. Specifically, after an initial increase, a sharp drop was recorded at 5 h for the cells exposed to toxic concentrations of digitoxin (i.e., 80 nM). A dramatic loss in cellular resistance was observed after about 10 h of exposure and was indicative of an acute effect of digitoxin on the cell adhesion or membrane impedance. Complementary, after an initial increase in the resistance of the cells exposed to 40 nM digitoxin, a gradual resistance drop was recorded starting at 8 h post-exposure. Further, 40 nM treated cells showed a smaller change in the resistance rate when compared to 80 nM digitoxin treated cells.

To correlate the observed apoptotic percentage with the real-time analysis of the resistance post-exposure to 40 and 80 nM digitoxin, we investigated cellular attachment. Our results showed that cells treated with 40 and 80 nM digitoxin exhibited a significant drop in α after 5 and 9 h of exposure, respectively (Fig. 4B). Our apoptotic data and previous experiments correlated such changes to the loss of cellular monolayer resulting from cell death and cell de-attachment (Arndt et al., 2004; Stolwijk et al., 2011). Contrary, cells exposed to 10 and 25 nM digitoxin showed a significant increase in α relative to controls, indicating a stimulation of their cellular attachment.

4. Discussion

We hypothesized that exposure to toxic, therapeutic and sub-therapeutic concentrations of digitoxin induces changes in NCI-H460 behavior that correlate with digitoxin's pharmacological profiles and can be analyzed in real-time. By combining standard cell viability and cell-based cytotoxicity assays, we showed that the percentage of apoptotic cells was both dose and time-dependent, with significant increases in the apoptotic percentage for the cells exposed to 25, 40 and 80 nM digitoxin and minor changes for the cells exposed to 10 nM relative to controls after 24 h exposure. Further, our results showed a dose-dependent decrease in the expression of key cell cycle regulatory protein CDK4 relative to control β-actin.

By exploiting the naturally evolved sensitivity of the cells and by using the cell as a primary transducer, we recorded the changes in cellular behavior as real time changes in cellular resistance and adhesion post-exposure to toxic, therapeutic and sub-therapeutic concentrations of digitoxin (Arndt et al., 2004; Chen et al., 2012). Our dynamic combinatorial analysis showed predominantly pro-apoptotic and anti-proliferative effects upon treatment with toxic and therapeutic concentrations of digitoxin (i.e., 80 and 40 nM) confirmed by a sharp drop in resistance. Complementary, the cells treated with sub-therapeutic concentrations of digitoxin (i.e., 25 and 10 nM) showed a hindered proliferation rate and increased cellular adhesion. Changes in α were directly related to the restrictions in the AC current caused by changes in the distance between the basal membrane and the ECIS electrodes. Cellular detachment and reduction in α post-exposure to 80 and 40 nM digitoxin were correlated to changes in nuclear morphology, cellular proliferation and cytotoxicity. Digitoxin's concentration-dependent changes illustrated the advantages of continuous monitoring provided by ECIS; in particular, the ECIS allowed for intermediate time events analysis identifying dramatic losses in cell resistance upon exposure to toxic concentrations of digitoxin and increases in the resistance of the cells exposed to sub-therapeutic concentrations. These differential cellular responses suggest the existence of threshold concentrations associated with either cellular mechanisms responsible for increased cellular adhesion or with a dose-dependent cellular inhibition coefficient profile of digitoxin.

Exposure to CGs is known to cause G1/S or G2 arrests in cancer cells at sub-cytotoxic levels (Perrone et al., 2012; Wang et al., 2012). Binding of nuclear CDK4 to cyclin D regulates retinoblastoma tumor suppressor (Rb) and E2F group expression that promotes G1/S phase transition (Berthet et al., 2006; Jia et al., 2006). Thus, therapeutic targeting of CDK4 in cancer cells has been proposed as an effective approach for cancer therapy (Puyol et al., 2010). Based on the decrease in CDK4 expression and real-time increase in cellular resistance upon exposure to 10 and 25 nM digitoxin, we hypothesize that digitoxin targets cellular adhesion by changing the subcellular distribution of CDK4 (Gulappa et al., 2013; Si and Liu, 2001) (Fig. 5). Our hypothesis is supported by previous studies that showed that reduction in the nuclear levels of CDK4 could result from CDK4 sequestration in the cytoplasm and CDK4 association with ZONAB (Balda and Matter, 2003). ZONAB is a Y-box transcription factor whose localization and transcriptional activity is regulated by the tight junction-associated candidate tumor suppressor and scaffolding protein zona occluding 1 (ZO-1) (Bauer et al., 2010; Kremerskothen et al., 2011). ZONAB binds to the Src homology 3 (SH3) binding domain of ZO-1 at the cell periphery (Tsukita, 2013; Vinken et al., 2011) and helps regulate paracellular permeability (Bauer et al., 2010; Itoh et al.,

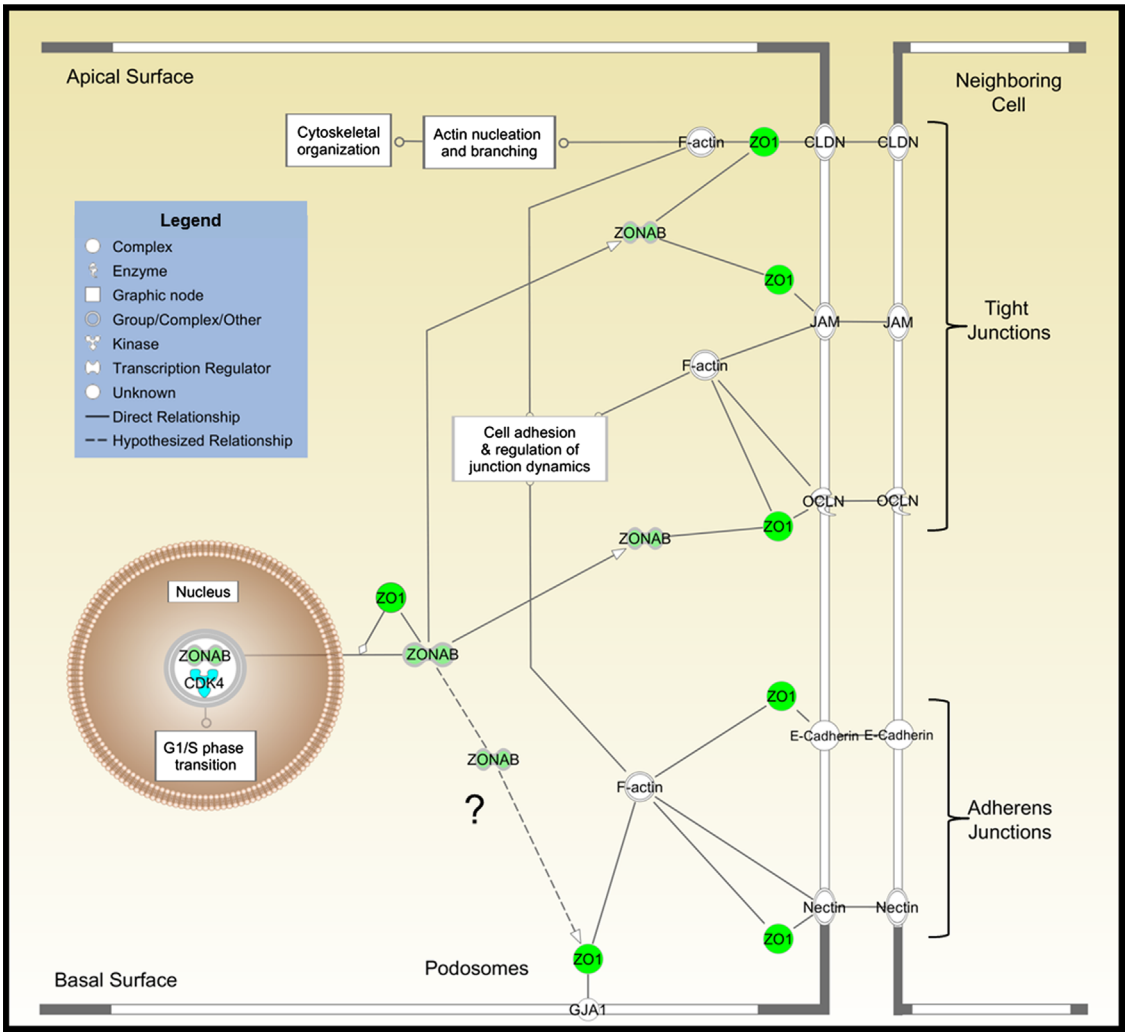

Fig. 5. Proposed cellular signaling pathways and regulatory effects between cellular proliferation and adhesion upon exposure to sub-therapeutic concentrations of digitoxin. Sequestration of CDK4 in cytoplasm by association with ZONAB regulates cell's junction dynamics.

1997) by its indirect participation in the formation of tight, adherent and gap junctions. ZO-1 interaction with the cytoplasmic domain of occludins (Li et al., 2005), junctional adhesion molecule (Mandell et al., 2006) and claudins (Cheung et al., 2012) regulates tight junction formation; additionally, ZO-1 interaction with E-cadherin (Priya et al., 2013) and nectine (Itoh et al., 1997; Muller et al., 2005) helps in the formation and maintenance of adherence junctions while ZO-1 interaction with gap junctions proteins (Abrams and Scherer, 2012; Bauer et al., 2010) regulates the formation of gap junctions. Given ZONAB's unaffected levels of expression upon cellular exposure to digitoxin (Supplementary information Fig. S2), the propensity of ZONAB to bind to ZO-1 and ZO-1's structural role in the basal podosomes biogenesis (Kremerskothen et al., 2011), it is also reasonable to assume that exposure to digitoxin leads to increased podosome formation that could enhance cell adhesion. Increasing ZO-1/ZONAB binding at the cell periphery, and subsequently the decrease in the nuclear levels of CDK4 levels would explain both the slow proliferation observed for the NCI-H460 cells exposed to 10 nM digitoxin as well as their higher adhesion.

Strengthening adhesion following exposure to sub-therapeutic concentrations of digitoxin could potentially alter actin nucleation/branching and thus cytoskeleton dynamics (González-Mariscal et al., 2007). Previous studies have shown that changes in adhesion and cell–cell contacts in neoplastic cells play a key role in cancer cell progression and metastasis regulation (Ni et al., 2013; van Nimwegen and van de Water, 2007). Such changes can further result in enhancement or re-establishment of the normal cellular function of the epithelial cells as well as re-establishment of cell-to-cell junctions (Coradini et al., 2011; Zhong and Rescorla., 2012).

Our results thus provide new evidence of digitoxin's potential role in regulating pro-adhesion through enhancement of CDK4/ZONAB/ZO-1 signaling as one of the basic mechanisms for controlling its anti-neoplastic effects. Our results are likely to open new avenues in which the suppression of such a signaling pathway might be broadly applied for the next generation of systematic screening of natural compounds with anti-cancer capabilities.

5. Conclusions

Our experimental approach intended to correlate the structural and morphological characteristics of cells exposed to digitoxin (as recorded by the ECIS system) with their functional and metabolic changes (as demonstrated using standard microscopy and cell biology assays). This correlation was made possible by the advantages of the ECIS system that allowed direct, continuously and noninvasively monitoring of NCI-H460 behavior before and after exposure to digitoxin. Our combinatorial analysis showed that exposure to toxic, therapeutic and sub-therapeutic concentrations

of digitoxin targets cancer cells in a dose and time-dependent manner. Specifically, toxic and therapeutic concentrations activate anti-proliferative cellular mechanisms, whereas sub-therapeutic concentrations of digitoxin increase cellular adhesion. Sequestering CDK4 in the cell cytoplasm reduces cancer cell progression. Understanding the underlying anti-neoplastic effects associated with exposure to digitoxin can expedite the potential implementation of this CG as a chemotherapeutic agent.

Acknowledgments

The authors acknowledge NanoSAFE and National Science Foundation/EPS-1003907 for their financial support and Applied Biophysics for the technical support.

Disclaimer: The findings and conclusions in this manuscript are those of the authors and do not necessarily represent the views of the National Institute for Occupational Safety and Health.

Appendix A. Supporting information

Supplementary data associated with this article can be found in the online version at http://dx.doi.org/10.1016/j.bios.2014.03.030.

References

Abrams, C.K., Scherer, S.S., 2012. Biochim. Biophys. Acta Biomembr. 1818 (8), 2030–2047.
Arndt, S., Seebach, J., Psathaki, K., Galla, H.-J., Wegener, J., 2004. Biosens. Bioelectron. 19 (6), 583–594.
Baggot, J.D., Davis, L.E., 1973. Res. Vet. Sci. 15 (1), 81–87.
Balda, M.S., Matter, K., 2003. Trends Cell Biol. 13 (6), 310–318.
Bauer, H., Zweimueller-Mayer, J., Steinbacher, P., Lametschwandtner, A., Bauer, H.C., 2010. J. Biomed. Biotechnol. 2010, 402593.
Berthet, C., Klarmann, K.D., Hilton, M.B., Suh, H.C., Keller, J.R., Kiyokawa, H., Kaldis, P., 2006. Dev. Cell 10 (5), 563–573.
Chen, S.-W., Yang, J.M., Yang, J.-H., Yang, S.J., Wang, J.-S., 2012. Biosens. Bioelectron. 33 (1), 196–203.
Cheung, I.D., Bagnat, M., Ma, T.P., Datta, A., Evason, K., Moore, J.C., Lawson, N.D., Mostov, K.E., Moens, C.B., Stainier, D.Y.R., 2012. Dev. Biol. 361 (1), 68–78.
Coradini, D., Casarsa, C., Oriana, S., 2011. Acta Pharmacol. Sin. 32 (5), 552–564.
Einbond, L.S., Shimizu, M., Ma, H., Wu, H.-a., Goldsberry, S., Sicular, S., Panjikaran, M., Genovese, G., Cruz, E., 2008. Biochem. Biophys. Res. Commun. 375 (4), 608–613.
Elbaz, H.A., Stueckle, T.A., Tse, W., Rojanasakul, Y., Dinu, C.Z., 2012a. Exp. Hematol. Oncol. 1 (1), 4.
Elbaz, H.A., Stueckle, T.A., Wang, H.-Y.L., O'Doherty, G.A., Lowry, D.T., Sargent, L.M., Wang, L., Dinu, C.Z., Rojanasakul, Y., 2012b. Toxicol. Appl. Pharmacol. 258 (1), 51–60.
Furukawa, K., Aida, T., Nonaka, Y., Osoda, S., Juarez, C., Horigome, T., Sugiyama, S., 2007. J. Struct. Biol. 160 (2), 125–134.
Giaever, I., Keese, C.R., 1984. Proc. Natl. Acad. Sci. U.S.A. 81 (12), 3761–3764.
Giaever, I., Keese, C.R., 1991. Proc. Natl. Acad. Sci. U.S.A. 88 (17), 7896–7900.
Giaever, I., Keese, C.R., 1993. Nature 366 (6455), 591–592.
González-Mariscal, L., Lechuga, S., Garay, E., 2007. Prog. Histochem. Cytochem. 42 (1), 1–57.
Gulappa, T., Reddy, R.S., Suman, S., Nyakeriga, A.M., Damodaran, C., 2013. Cancer Lett. 337 (2), 177–183.
Ho, A.K., Ceña, V., Klein, D.C., 1987. Biochem. Biophys. Res. Commun. 142 (3), 819–825.
Itagaki, K., Adibnia, Y., Sun, S., Zhao, C., Sursal, T., Chen, Y., Junger, W., Hauser, C.J., 2011. Shock 36 (6), 548–552.
Itoh, M., Nagafuchi, A., Moroi, S., Tsukita, S., 1997. J. Cell Biol. 138 (1), 181–192.
Jagielska, J., Salguero, G., Schieffer, B., Bavendiek, U., 2009. Atherosclerosis 206 (2), 390–396.
Jia, X., Liu, B., Shi, X., Gao, A., You, B., Ye, M., Shen, F., Du, H., 2006. Cell Biol. Int. 30 (2), 183–189.
Kremerskothen, J., Stolting, M., Wiesner, C., Korb-Pap, A., van Vliet, V., Linder, S., Huber, T.B., Rottiers, P., Reuzeau, E., Genot, E., Pavenstadt, H., 2011. FASEB J. 25 (2), 505–514.
Larre, I., Lazaro, A., Contreras, R.G., Balda, M.S., Matter, K., Flores-Maldonado, C., Ponce, A., Flores-Benitez, D., Rincon-Heredia, R., Padilla-Benavides, T., Castillo, A.d., Shoshani, L., Cereijido, M., 2010. Proc. Natl. Acad. Sci. U.S.A. 107 (25), 11387–11392.
Li, Y., Fanning, A.S., Anderson, J.M., Lavie, A., 2005. J. Mol. Biol. 352 (1), 151–164.
López-Lázaro, M., 2007. Expert Opin. Ther. Targets 11 (8), 1043–1053.
Lopez-Lazaro, M., Pastor, N., Azrak, S.S., Ayuso, M.J., Austin, C.A., Cortes, F., 2005. J. Nat. Prod. 68 (11), 1642–1645.
López-Lázaro, M., Pastor, N., Azrak, S.S., Ayuso, M.J., Cortés, F., Austin, C.A., 2006. Leuk. Res. 30 (7), 895–898.
Mandell, K.J., Holley, G.P., Parkos, C.A., Edelhauser, H.F., 2006. Invest. Ophthalmol. Visual Sci. 47 (6), 2408–2416.
Melnikova, V.O., Balasubramanian, K., Villares, G.J., Dobroff, A.S., Zigler, M., Wang, H., Petersson, F., Price, J.E., Schroit, A., Prieto, V.G., Hung, M.-C., Bar-Eli, M., 2009. J. Biol. Chem. 284 (42), 28845–28855.
Menger, L., Vacchelli, E., Kepp, O., Eggermont, A., Tartour, E., Zitvogel, L., Kroemer, G., Galluzzi, L., 2013. Oncoimmunology 2 (2), e23082.
Mijatovic, T., Mathieu, V., Gaussin, J.F., De Neve, N., Ribaucour, F., Van Quaquebeke, E., Dumont, P., Darro, F., Kiss, R., 2006a. Neoplasia 8 (5), 402–412.
Mijatovic, T., Op De Beeck, A., Van Quaquebeke, E., Dewelle, J., Darro, F., de Launoit, Y., Kiss, R., 2006b. Mol. Cancer Ther. 5 (2), 391–399.
Muller, S.L., Portwich, M., Schmidt, A., Utepbergenov, D.I., Huber, O., Blasig, I.E., Krause, G., 2005. J. Biol. Chem. 280 (5), 3747–3756.
Newman, R.A., Yang, P., Pawlus, A.D., Block, K.I., 2008. Mol. Interventions 8 (1), 36–49.
Ni, J., Cozzi, P., Hao, J., Beretov, J., Chang, L., Duan, W., Shigdar, S., Delprado, W., Graham, P., Bucci, J., Kearsley, J., Li, Y., 2013. Int. J. Biochem. Cell Biol. 45 (12), 2736–2748.
Perrone, A., Capasso, A., Festa, M., Kemertelidze, E., Pizza, C., Skhirtladze, A., Piacente, S., 2012. Fitoterapia 83 (3), 554–562.
Pongrakhananon, V., Stueckle, T.A., Wang, H.-Y.L., O'Doherty, G.A., Dinu, C.Z., Chanvorachote, P., Rojanasakul, Y., 2014. Biochem. Pharmacol. 88, 23–35.
Prassas, I., Karagiannis, G.S., Batruch, I., Dimitromanolakis, A., Datti, A., Diamandis, E.P., 2011. Mol. Cancer Ther. 10 (11), 2083–2093.
Priya, R., Yap, A.S., Gomez, G.A., 2013. Differentiation 86 (3), 133–140.
Puyol, M., Martín, A., Dubus, P., Mulero, F., Pizcueta, P., Khan, G., Guerra, C., Santamaría, D., Barbacid, M., 2010. Cancer Cell 18 (1), 63–73.
Sapper, A., Wegener, J., Janshoff, A., 2006. Anal. Chem. 78 (14), 5184–5191.
Si, X., Liu, Z., 2001. Oral Oncol. 37 (5), 431–436.
Spegel, C., Heiskanen, A., Skjolding, L.H.D., Emnéus, J., 2008. Electroanalysis 20 (6), 680–702.
Stolwijk, J.A., Hartmann, C., Balani, P., Albermann, S., Keese, C.R., Giaever, I., Wegener, J., 2011. Biosens. Bioelectron. 26 (12), 4720–4727.
Storstein, L., Nore, A.K., Sjaastad, O., 1979. Clin. Cardiol. 2 (2), 146–150.
Sun, K., Halberg, N., Khan, M., Magalang, U.J., Scherer, P.E., 2013. Mol. Cell Biol. 33 (5), 904–917.
Tsukita, S., 2013. In: Lennarz, W.J., Lane, M.D. (Eds.), Encyclopedia of Biological Chemistry. Academic Press, Waltham, pp. 392–395
van Nimwegen, M.J., van de Water, B., 2007. Biochem. Pharmacol. 73 (5), 597–609.
Vinken, M., Decrock, E., De Vuyst, E., Ponsaerts, R., D'Hondt, C., Bultynck, G., Ceelen, L., Vanhaecke, T., Leybaert, L., Rogiers, V., 2011. Biochim. Biophys. Acta Rev. Cancer 1815 (1), 13–25.
Wang, H.-Y.L., Xin, W., Zhou, M., Stueckle, T.A., Rojanasakul, Y., O'Doherty, G.A., 2010. ACS Med. Chem. Lett. 2 (1), 73–78.
Wang, H.S., Keese, C.R., Giaever, I., Smith, T.J., 1995. J. Clin. Endocrinol. Metab. 80 (12), 3553–3560.
Wang, Y., Qiu, Q., Shen, J.-J., Li, D.-D., Jiang, X.-J., Si, S.-Y., Shao, R.-G., Wang, Z., 2012. Int. J. Biochem. Cell Biol. 44 (11), 1813–1824.
Wegener, J., Hakvoort, A., Galla, H.-J., 2000a. Brain Res. 853 (1), 115–124.
Wegener, J., Keese, C.R., Giaever, I., 2000b. Exp. Cell Res. 259 (1), 158–166.
Winnicka, K., Bielawski, K., Bielawska, A., 2006. Acta Pol. Pharm. 63 (2), 109–115.
Wu, S.L., Li, W., Wells, A., Dasgupta, A., 2001. Am. J. Clin. Pathol. 115 (4), 600–604.
Xiao, C., Luong, J.H.T., 2005. Toxicol. Appl. Pharmacol. 206 (2), 102–112.
Xie, Z., Cai, T., 2003. Mol. Interventions 3 (3), 157–168.
Yuan, B.-Z., Jefferson, A.M., Millecchia, L., Popescu, N.C., Reynolds, S.H., 2007. Exp. Cell Res. 313 (18), 3868–3880.
Zhong, X., Rescorla, F.J., 2012. Cell. Signal. 24 (2), 393–401.